THE JOURNAL OF PHYSICAL CHEMISTRY B

Article

pubs.acs.org/JPCB

Origin of Long-Lived Coherences in Light-Harvesting Complexes

Niklas Christensson,[†] Harald F. Kauffmann,[†,⊥] Tõnu Pullerits,[‡] and Tomáš Mančal*[,§]

[†]Faculty of Physics, University of Vienna, Strudlhofgasse 4, 1090 Vienna, Austria

[‡]Department of Chemical Physics, Lund University, P.O. Box 124, SE-22100 Lund, Sweden

[§]Faculty of Mathematics and Physics, Charles University in Prague, Ke Karlovu 5, Prague 121 16, Czech Republic

[⊥]Faculty of Physics, Vienna University of Technology, 1040 Vienna, Austria

ABSTRACT: A vibronic exciton model is applied to explain the long-lived oscillatory features in the two-dimensional (2D) electronic spectra of the Fenna–Matthews–Olson (FMO) complex. Using experimentally determined parameters and uncorrelated site energy fluctuations, the model predicts oscillations with dephasing times of 1.3 ps at 77 K, which is in a good agreement with the experimental results. These long-lived oscillations originate from the coherent superposition of vibronic exciton states with dominant contributions from vibrational excitations on the same pigment. The oscillations obtain a large amplitude due to excitonic intensity borrowing, which gives transitions with strong vibronic character a significant intensity despite the small Huang–Rhys factor. Purely electronic coherences are found to decay on a 200 fs time scale.

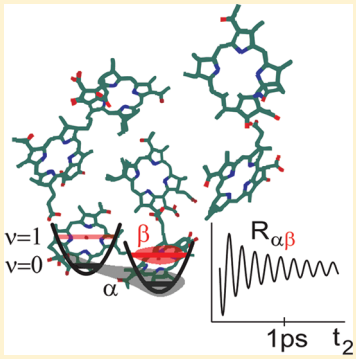

INTRODUCTION

The role of quantum mechanics in biological processes, as well as photosynthetic light-harvesting, has been of interest for a long time.[1−3] The topic received renewed attention after the observation of long-lived oscillations in the two-dimensional (2D) spectra of the Fenna–Matthews–Olson (FMO) protein pigment complex.[4] These oscillations were interpreted as a signature of electronic coherences between the delocalized energy eigenstates of the complex, and it was argued that their slow dephasing could enhance the efficiency of energy transfer between the chlorosome antenna and the reaction center.[4,5] Subsequent studies revealed that the oscillations in FMO have a dephasing time of 1.2 ps at 77 K,[6] and that such oscillations are a common feature of light-harvesting complexes.[7,8] On the basis of the known structure of FMO,[1] simulations employing formally exact equations of motions for the reduced density operator found oscillations with dephasing times of 200−300 fs—clearly shorter than the experimental observation.[5,9−11] Significantly longer dephasing times were found if the transition frequency fluctuations (static or dynamic) of the different pigments are assumed to be correlated.[12,13] However, theoretical studies using molecular dynamics simulations of the interaction between electronic and nuclear degrees of freedom (DOF) have not been able to confirm the existence of such correlations.[14,15] To what extent the long-lived oscillations in the experiments reflect electronic coherences, or if they influence the transport of energy across the complex, thus remains an open question.

Analysis of excitation dynamics in molecular aggregates typically employs a reduced description, where the electronic DOF and their mutual couplings are treated explicitly, and the nuclear modes of the pigments and protein are treated as a heat bath.[16,17] The presence of underdamped vibrational modes in the bath produces oscillatory signatures in 2D spectra which are similar to the modulations predicted for electronic coherences.[18] The dephasing time of such nuclear coherence are of the order of several picoseconds, and they can often be treated as completely undamped on the time scale of a typical 2D experiment. Low temperature fluorescence line narrowing (FLN) experiments on FMO have revealed a large number of vibrational modes in the range of 0−350 cm^{-1}.[19,20] Time resolved measurements have shown that low frequency vibrational coherences in BChls have dephasing times on the order of a few ps.[21] However, the oscillations seen in the 2D spectra of FMO cannot be directly related to simple nuclear wavepackets, because the frequency of the oscillations does not match any of the vibrational frequencies, and the Huang–Rhys factors of the modes are too low. On the other hand, recent simulations have revealed unexpected effects on the electronic structure and dynamics if vibrational modes are explicitly included in the system.[22−24] Motivated by these results, we apply a vibronic exciton Hamiltonian in the one particle approximation[25−27] to FMO, in which one vibrational mode on each monomer is treated explicitly. Including significant vibrational modes explicitly into system enables us to avoid approximations which would otherwise arise from their perturbative treatment as members of the bath. In addition, it justifies the usage of a less advanced method in treatment of the system–bath coupling. We will show below that this model predicts oscillations in the 2D spectra of FMO with 1.3 ps dephasing times at 77 K and that they can be traced to coherent superpositions of vibronic exciton states located on the same pigment.

Received: May 14, 2012
Published: May 29, 2012

   dx.doi.org/10.1021/jp304649c | J. Phys. Chem. B 2012, 116, 7449−7454

MODEL

The total Hamiltonian of a molecular aggregate in contact with the environment is partitioned in a standard way into system, bath and system-bath interaction terms, $H = H_S + H_B + H_{SB}$. The system Hamiltonian describes the Q_y transition on each bacteriochlorophyll (BChl) in FMO (Figure 1) with the vibrational progression of a single vibrational mode. Including the resonance coupling between the transitions, the system Hamiltonian reads

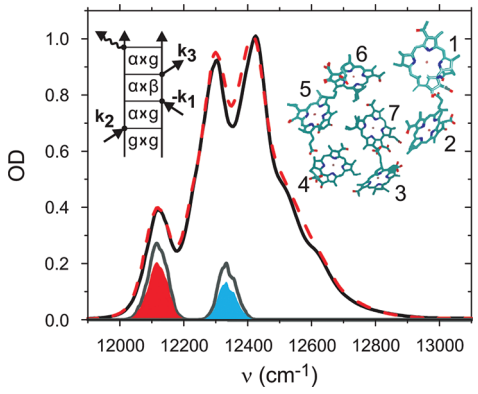

Figure 1. Linear absorption spectrum at 77 K for the exciton model (black) and the vibronic exciton model (red dash). The gray lines show the distribution of renormalized transition frequencies weighted by the transition strength (scaled by 2/3) for state 1 and 4 in the vibronic exciton model. The filled areas illustrate the relative contribution from electronic (red) and vibronic (blue) excitations on pigment 3. The spectra of the vibronic exciton model have been shifted by the reorganization energy of the vibrational mode (−9.25 cm^{-1}) for comparison. The insets show the Feynman diagram illustrating the nonrephasing excited state coherence pathway in state 5, and the arrangement of the 7 BChls in FMO (*C. tepidum*).[30] This figure was generated using the VMD software.[31]

$$H_S = \sum_{n,\nu,m,\nu'} [\delta_{nm}\delta_{\nu\nu'}(E_n + \nu\hbar\omega_0) + J_{n,\nu;m,\nu'}]|n,\nu\rangle\langle m,\nu'| \quad (1)$$

where E_n is the transition frequency of pigment n (site energy), ω_0 is the vibrational frequency, and ν is the quantum number of the vibrational mode. The coupling energy $J_{n,\nu;m,\nu'}$ between the individual transitions can be expressed via the electronic resonance coupling J_{nm}[17] and the Franck−Condon amplitudes of the vibrational mode[26] $J_{n,\nu;m,\nu'} = J_{nm}\langle\nu|0\rangle\langle\nu'|0\rangle$. The eigenvalues and wave functions of H_S are given by $\hbar\omega_\alpha$ and $|\alpha\rangle = \sum_{n,\nu}c^\alpha_{n,\nu}|n,\nu\rangle$, respectively. The bath Hamiltonian, H_B, is described as a collection of independent harmonic oscillators, for which the system-bath interaction is given by $H_{SB} = \sum_{n,\nu}\hbar\omega d_n(\omega)\tilde{q}_n|n,\nu\rangle\langle n,\nu|$. Here $\tilde{q}$ is a generalized coordinate of the environment, and $d(\omega)$ is the displacement of the excited state vibrational potential relative to the ground state. We assume that the system−bath Hamiltonian does not depend on the state of the vibrational mode (ν), implying that a vibrational coherence on an isolated monomer is undamped. Assuming equal but uncorrelated system-bath interaction for the different pigments, the energy gap correlation function in the local basis is given by $C_{nm}(t) = \hbar^2\omega^2 d_n d_m\langle\tilde{q}_n(t)\tilde{q}_m(0)\rangle = C_0(t)\delta_{nm}$. When the interaction of the system with the environmental modes (i.e., all except those treated explicitly in the system Hamiltonian) is weak, it is advantageous to perform calculations in the eigenstate basis of the system Hamiltonian. The correlation function of the energy gap in the eigenstate representation can be expressed via the expansion coefficients, $c^\alpha_{n,\nu}$, and the correlation function of each excitation in the local basis $C_0(t)$,

$$\begin{aligned} C_{\alpha\beta}(t) &= C_0(t)\{\sum_{n,\nu}(c^\alpha_{n,\nu})^2(c^\beta_{n,\nu})^2 \\ &\quad + \sum_{n,\nu\neq\nu'}[(c^\alpha_{n,\nu})^2(c^\beta_{n,\nu'})^2 + (c^\alpha_{n,\nu'})^2(c^\beta_{n,\nu})^2]\} \\ &= C_0(t)\gamma_{\alpha\beta} \end{aligned} \quad (2)$$

The dephasing dynamics of a coherent superposition between the eigenstates α and β is determined by the line shape function $g_{\alpha\beta}(t) = \int_0^t d\tau \int_0^\tau d\tau' \gamma_{\alpha\beta}C_0(\tau')$. The correlation function $C_0(t)$ is connected to the spectral density $\tilde{C}''(\omega)$ via a Fourier transform.[28] In addition to dephasing, the system-bath interaction leads to relaxation between the eigenstates of the system. Previous works have shown that the population relaxation rates obtained using Redfield and modified Redfield theory for FMO are similar.[17] Here, we use Redfield theory[16] (Markov and secular approximation), where the relaxation rate is given by

$$\begin{aligned} k_{\alpha\to\beta} = 2\pi \sum_{m,\nu,\nu'} c^\alpha_{m,\nu}c^\alpha_{m,\nu'}c^\beta_{m,\nu}c^\beta_{m,\nu'} \times \{(1 + n(\omega_{\alpha\beta}))\tilde{C}''(\omega_{\alpha\beta}) + n(-\omega_{\alpha\beta})\tilde{C}''(-\omega_{\alpha\beta})\} \end{aligned} \quad (3)$$

where $\tilde{C}''(\omega_{\alpha\beta}) > 0$ and $n(\omega_{\alpha\beta})$ is the Bose−Einstein distribution function. The total relaxation rate from a level α, $\Gamma_\alpha = (1/2)\sum_{\gamma\neq\alpha}k_{\alpha\to\gamma}$, determines the lifetime broadening of this exciton state. Assuming $k_BT < \hbar\omega_0$, the linear absorption spectrum can be calculated as[17]

$$OD(\omega) \propto \omega\langle\sum_\alpha |\mu_{\alpha 0}|^2 \mathrm{Re}\int_0^\infty dt\, e^{-g_{\alpha\alpha}(t)-\Gamma_\alpha t - i(\omega_{\alpha 0}-\omega)t}\rangle_{\Delta,\Omega} \quad (4)$$

where α runs over all exciton levels and the transition dipole moments $\mu_{\alpha 0}$ are given by $\mu_{\alpha 0} = \sum_{n,\nu}c^\alpha_{n,\nu}\mu_n\langle\nu|0\rangle$. Here $\langle\ldots\rangle_{\Delta,\Omega}$ denotes the average over a random distribution of pigment energies and orientations of complexes.

To simulate the oscillations in a third order experiment (i.e., 2D spectra) we adopt the doorway window representation.[29] Of all Liouville pathways contributing to the signal, only those involving a coherence between two levels in the excited state will give rise to oscillations during the waiting time t_2. Without loss of generality, we focus on the nonrephasing coherence pathways illustrated in Figure 1, which give rise to oscillations along the diagonal in the nonrephasing 2D spectrum.[7] The response function for this pathway is given by

$$R_{\alpha\beta,0} = \langle\langle(\mu_{\alpha 0})^2(\mu_{\beta 0})^2\rangle_\Omega G_\alpha(t_3)G^{(2)}_{\alpha\beta}(t_2)G_\alpha(t_1)\rangle_\Delta \quad (5)$$

where $G_\alpha(t) = e^{-i\omega_{\alpha 0}t-\Gamma_\alpha t-g_{\alpha\alpha}(t)}$, and $G^{(2)}_{\alpha\beta}(t_2) = e^{-i\omega_{\alpha\beta}t_2}\, e^{-g_{\alpha\alpha}(t_2)-g_{\beta\beta}(t_2)+g_{\alpha\beta}(t_2)-(\Gamma\alpha+\Gamma\beta)t_2}$. In this work we use the site energies (E_n) and resonance couplings (J_{nm}) for FMO *Chlorobium tepidum*, and the analytical formula for the overdamped part of the spectral density, $\tilde{C}''(\omega)$,[17] extracted from a FLN experiment.[19] The direction of the transition dipole moments were taken from the Protein Data Bank file 3ENI.[30] FLN experiments have identified a large number of low frequency vibrational modes in FMO, and the strongest feature in the spectrum arises from three modes around 185 cm^{-1}.[19] To retain a simple description,

dx.doi.org/10.1021/jp304649c | J. Phys. Chem. B 2012, 116, 7449−7454

we treat this cluster of modes as one effective mode with a frequency of $\omega_0 = 185$ cm^{-1} and a Huang−Rhys factor of 0.05. For calculations within the exciton model, this vibrational mode was included in the spectral density as an underdamped mode with 10 ps dephasing time. In all calculations presented in this paper, we sampled the pigment transition energies from a Gaussian distribution with a fwhm of 80 cm^{-1}.

DISCUSSION

Exciton and Vibronic-Exciton Coherences in FMO. The vibronic exciton and exciton model predict very similar linear optical properties as illustrated by the simulated linear absorption spectra shown in Figure 1. Figure 2a shows the

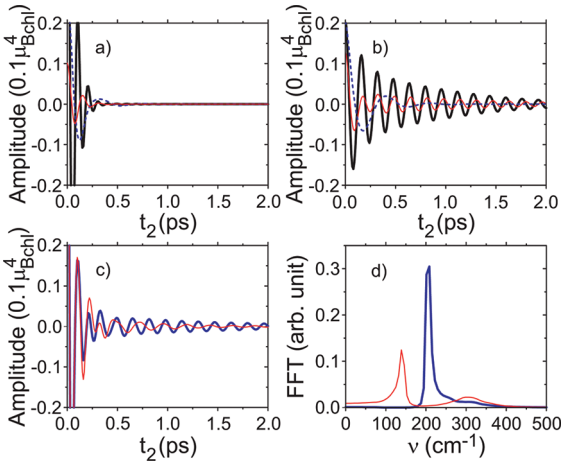

Figure 2. Amplitude of the real part of the nonrephasing coherence pathways involving the lowest state. $Re\langle R_{1\beta}\rangle_{\Omega,\Delta}$ with $\beta = 2$ (blue dash), $\beta = 3$ (red thin solid), and $\beta = 4$ (black solid) for the exciton model (a) and vibronic exciton model (b). (c) Sum of all nonrephasing coherence pathways, $\sum_{\alpha\beta} Re\langle R_{\alpha\beta}\rangle_{\Omega\Delta}$, giving rise to signal in the range 12100 ± 30 cm^{-1} for the vibronic exciton model with $\omega_0 = 185$ cm^{-1} (blue) and $\omega_0 = 117$ cm^{-1} (red) at 77 K. The initial value of the signal is 0.48 and the first minimum at $t_2 = 0.04$ ps has an amplitude of −0.23. The nonrephasing stimulated emission signal calculated for the same parameters and spectral range has an initial value of 0.17. (d) Power spectrum of the Fourier transform of the signals in part c starting from 0.2 ps.

time evolution of coherence pathways involving the lowest state of the exciton model. During t_2 the signals oscillate with frequencies corresponding to the splitting between the exciton levels, and they are completely damped after 400 fs. The exciton model in this work only results in somewhat shorter dephasing times than models including both nonsecular and non-Markovian effects (*vide supra*). We can thus conclude that inclusion of these effects is not sufficient to explain the ps dephasing times seen in the experiments.

The electronic exciton coherences experience both homogeneous and inhomogeneous dephasing, and this model cannot account for the dephasing time of the oscillations when the transition frequency fluctuations of different pigments are uncorrelated (see Figure 2). The strong homogeneous dephasing can be understood from eqs 3 and 5. For the exciton model we find that the cross-correlation term $g_{\alpha\beta}$ is small and the coherence pathways decay mainly with $\exp(-g_{\alpha\alpha}(t_2) - g_{\beta\beta}(t_2))$. For the experimentally determined spectral density used in this work, $\exp(-g_{\alpha\alpha}(t_1))$ decays on 140 fs time scale. The presence of correlated transition frequency fluctuations of different pigments would result in larger cross-correlation terms in eq 5 and longer homogeneous dephasing times. However, numerical simulations have found that the uncorrelated bath approximation employed here is indeed valid for FMO (i.e., no correlation of transition frequency fluctuations of different pigments).[14] Furthermore, even if such dynamic correlations would be present, the inhomogeneous dephasing due to the distribution of pigment energies would limit the dephasing time of the oscillations to about 200 fs. Coherence with ps dephasing time in the electronic model thus requires a correlation of both dynamic fluctuations *and* static distributions of the transition energies of different pigments.

The oscillations resulting from the coherence pathways involving the lowest levels of the vibronic exciton model are shown in Figure 2b. The oscillations are remarkably long-lived, and the signal continues to oscillate beyond 2 ps. The long dephasing time of the coherences in the vibronic exciton model can be understood by inspection of the expansion factors $\langle |c^{\alpha}_{n,\nu}|^2\rangle_{\Delta}$ given in Figure 1 and the transition frequency distributions shown in Table 1. For instance, state 1

Table 1. Contributions of Selected Basis Excitations ($|c^{\alpha}_{n,\nu}|^2$) to the Four First Vibronic Exciton States Averaged over Energetic Disorder ($\omega_0 = 185$ cm^{-1})[a]

$\langle |c^{\alpha}_{n,\nu}|^2\rangle_{\Delta}$	$\alpha = 1$	$\alpha = 2$	$\alpha = 3$	$\alpha = 4$
$n = 1, \nu = 0$	0.0	0.03	0.58	0.15
$n = 1, \nu = 1$	0.0	0.0	0.0	0.0
$n = 3, \nu = 0$	0.75	0.2	0.03	0.0
$n = 3, \nu = 1$	0.0	0.0	0.2	0.67
$n = 4, \nu = 0$	0.21	0.51	0.01	0.01
$n = 4, \nu = 1$	0.0	0.0	0.0	0.01
$\langle \mu_{\alpha}^2\rangle_{\Delta}\langle \mu_{BChl}^2\rangle$	0.87	0.58	1.3	0.57
$\langle E_{\alpha}\rangle_{\Delta} - \langle E_1\rangle_{\Delta}$ (cm^{-1})	0.0	105	175	217

[a]The numbering of the pigments is defined in Figure 1. The two bottom rows show the averaged transition strength in units of the BChl monomer, and the average energy differences between the vibronic exciton levels, respectively.

corresponds to 75% to an excitation of the $\nu = 0$ transition of pigment 3, while state 4 has a large contribution of vibrational excitation ($\nu = 1$) on the same pigment. As discussed above, the system-bath interaction is independent of the state of the vibrational mode, and these two vibronic exciton levels will therefore experience highly correlated fluctuations. This type of correlation leads to slow homogeneous dephasing of coherences with large "intrapigment" character. Despite the large contribution from the vibrational excitation to state 4, it has a transition dipole moment which is comparable to that of the other vibronic exciton levels. For noninteracting pigments, only the zero-phonon state ($\nu = 0$) has a significant transition dipole moment. The strong transition dipole moment here is the result of intensity borrowing from the electronic transitions on the other pigments. By comparison to the stimulated emission signal calculated for the same spectral range, we estimate the modulation of the total signal, including stimulated emission and ground state bleach, to be approximately 5% for $t_2 > 0.3$ ps.

Figure 2c shows the oscillations (due to all pathways) on the red edge of the linear absorption spectrum for the vibronic exciton model. The oscillations show a biphasic behavior, where the initial 200 fs decay of the oscillation is due to the decay of

dx.doi.org/10.1021/jp304649c | J. Phys. Chem. B 2012, 116, 7449−7454

coherences between vibronic exciton states localized on different pigments (like the coherence between states 1 and 2 in the vibronic exciton model, Figure 2b and Table 1), while the long-lived oscillations reflect coherences between vibronic exciton states localized on the same pigment ("intrapigment"). A fit to the oscillations gives a dephasing time of 1.3 ps.

The Fourier transform of the signal in Figure 2c is shown in Figure 2d. The oscillation frequency of 205 cm^{-1} is higher than ω_0 and also higher than the frequency observed in the experiment (160 cm^{-1}).[6] The oscillation frequency depends on transition energies, electronic couplings and vibrational frequencies according to eq 1. Parts c and d of Figure 2 compare the oscillations on the red edge of the spectrum for two different vibrational frequencies found in the FLN experiment, ω_0 = 185 cm^{-1} and ω_0 = 117 cm^{-1}. For ω_0 = 117 cm^{-1}, the oscillations have a frequency of 140 cm^{-1} and a shorter dephasing time as compared to ω_0 = 185 cm^{-1}. The dephasing time of the oscillations depends on the amount of vibrational character of the vibronic exciton states, and detailed analysis of the oscillations provide information on the energies and nature of the eigenstates not accessible from linear spectra (Figure 1). Vibronic exciton coherences can easily be distinguished from the wavepackets enabled by the vibrational modes in the ground state. Ground state wavepackets have frequencies which are identical to that of the vibrational modes, and we find that their amplitudes are approximately an order of magnitude weaker than the vibronic exciton coherences for the present set of parameters.

The "intrapigment" nature of specific coherences in the vibronic exciton model leads to slow homogeneous dephasing because of the inherent correlation of the transition frequency fluctuations of vibrational transitions on the same pigment. This type of correlation is caused by an effective decoupling of the vibrational modes from the harmonic bath of normal modes, and corresponds to the long-lived vibrational coherences observed in BChl monomers.[21] Furthermore, those vibronic exciton states which are dominated by transitions located on the same pigment experience correlated shifts when the pigment energies are sampled from a random distribution, and are thus quite insensitive to the width of the inhomogeneous distribution. The "intrapigment" coherences in the vibronic exciton model thus experience only a weak homogeneous *and* inhomogeneous dephasing. To achieve the same properties of the coherences in the electronic model, one needs to postulate a correlation of environment induced fluctuations (and distributions) as an independent assumption. Thus, what is realized by an assumption in the electronic model, is in the vibronic model a direct consequence of the experimentally verified property of intramolecular vibrational modes.

Long-Lived Oscillations in Modified FMO Complexes. Recently, Hayes et al.[6] investigated the long-lived oscillations in a series of modified FMO complexes. It was found that the oscillations were identical for the native complex, a mutant with altered hydrocarbon tails and for inhomogeneously deuterated FMO complexes. For the inhomogeneously deuterated sample, a normal-mode analysis was carried out which indicated that the normal mode with frequency closest to the observed oscillation frequency (158 cm^{-1}) experienced a shift and inhomogeneous broadening (approximately 20 cm^{-1}). No mode in this spectral range was detected in the FLN experiments,[19] indicating that such a mode has a low S-factor. An extensive resonance Raman study on the accessory BChl[32] found a weak mode with a frequency of 160 cm^{-1}, and assigned it to the in-plane deformation of $C_{acetyl}-CH_3$, which would explain the strong sensitivity to deuteration. The modes with larger S-factor around 117 and 185 cm^{-1} (seen in FLN and used in this work) were assigned to in-plane C_2-C_{acetyl} deformation and out-of-plane deformations of the pyrrole rings, respectively. A more recent study assigned the 185 cm^{-1} mode to the deformation of the pyrrole rings and the central Mg atom.[33] Both these studies show that the modes with large S-factor do not directly involve the motions of hydrogen atoms or the hydrocarbon tail, and are thus not expected to shift significantly due to deuteration or to change for the mutant. To what extent the modes with significant Huang–Rhys factors experience inhomogeneous broadening upon partial deuteration is thus unclear, and should be investigated by frequency-(resonance Raman or FLN) or time-resolved measurements on the dueterated BChl monomers. Like the presence of any inhomogeneity (e.g., pigment energies in the exciton model), an uncorrelated distribution of vibrational frequencies will lead to an inhomogeneous dephasing contribution in the vibronic exciton model. However, the inhomogeneous dephasing component of the vibronic exciton coherences is different from that of a wavepacket (i.e., a convolution with the distribution of vibrational frequencies). For vibronic excitons, a change in the vibrational frequency leads to simultaneous changes in the transition dipole moments, energies and "character" of the states. This leads to an effect similar to motional narrowing known from the exciton model (i.e., the ihomogeneous distribution is narrowed). The details of this process require further investigations, but preliminary results indicate that this effect may substantially reduce the inhomogeneous dephasing for vibronic exciton coherences, especially when more than one vibrational mode is included in the system Hamiltonian.

For the FMO mutant with modified hydrocarbon tails, the linear absorption spectrum reveals significant broadening band accompanied by a loss of intensity of the band at 12350 cm^{-1}.[6] The broadening of the lowest transition indicates a significant increase in the inhomogeneous broadening (on the order of 50%). However, increasing the inhomogeneous broadening is not sufficient to explain the decrease in intensity of the band at 12350 cm^{-1}. To account for the spectrum of the mutant, additional changes in the site energies, couplings, local system-bath interaction or inhomogeneous broadening of the pigments responsible for the high energy absorption are required. The large change in the band around 12350 cm^{-1} is particularly interesting. In the electronic model, this band is the "upper state" involved in the coherence oscillating with a frequency of 160 cm^{-1}. In the context of the exciton model, it is not clear how a large change in this band can be consistent with an unchanged dephasing of the coherence. Furthermore, the observed oscillations do not change despite the significant increase in inhomogeneous broadening. In the context of the electronic coherence model this means that the correlation of the site energy inhomogeneous distribution, which is necessary to overcome the inhomogeneous dephasing, has to increase in the mutant.

For the vibronic exciton model, the states involved in the long-lived coherence are located on the pigment with lowest energy, and are thus largely insensitive to changes involving the pigments responsible for the absorption at higher frequencies. As can be seen from Figure 1, the upper state (state 4) is not the main contributor to the absorption at 12350 cm^{-1}, and a

change in this band is not a signature of a change in the vibronic exciton states involved in the long-lived coherence. The vibronic exciton model also provides a straightforward explanation of the insensitivity of the oscillations to the increased inhomogeneous broadening in the mutant. The long-lived oscillations arise from "intrapigment" coherences, which are weakly sensitive to the inhomogeneous distribution of transition energies.

CONCLUSIONS

In this work, we have shown that the vibronic exciton model predicts oscillation in the 2D spectra of FMO with 1.3 ps dephasing times at 77 K. Our model does not invoke static nor dynamic correlations in the site energies of the pigments, and uses experimentally determined spectral densities and vibrational frequencies. The long-lived oscillations are found to reflect coherent superpositions of vibronic exciton states with dominant contributions from vibrational excitations on the same pigment. Such "intrapigment" coherences experience weak homogeneous and inhomogeneous dephasing due to the inherent correlation of transition frequency fluctuations of the involved states. Because vibrational modes are an inherent property of all pigments, we expect vibronic excitons to be a general feature in the dynamics of molecular aggregates. In the exciton language, the long-lived oscillations reported here correspond to a coherence between the system and the bath. Because the resonance coupling in the vibronic exciton model acts on the system as well as on certain vibrational modes (eq 1), both types of DOF become mixed. A similar mixing of system and vibrational DOF takes place implicitly when the reduced equation of motion for the electronic system is propagated exactly.[34] In general, this type of mixing takes place for all nuclear modes. However, modes of the protein environment are strongly damped and cannot contribute to a long dephasing time. As shown here, one or more of the underdamped vibrations found in the BChl monomers are needed to account for the dephasing times of the coherences. Recent experiments have shown that there is more than one long-lived oscillation component in FMO.[35] In the context of the vibronic exciton model, such observations can be qualitatively understood from the multiple Franck−Condon active low frequency vibrational modes present in the monomers.[19,21,32]

The strong mixing of electronic and vibrational DOF which enables long-lived oscillation in the 2D spectra of FMO will most likely influence the energy transfer dynamics in the complex. However, our results show that the oscillations themselves mostly reflect the dynamics of nuclear DOF within one pigment, and they should therefore provide little information about the transfer of energy from the chlorosome to the reaction center.

AUTHOR INFORMATION

Corresponding Author

*E-mail: mancal@karlov.mff.cuni.cz.

Notes

The authors declare no competing financial interest.

ACKNOWLEDGMENTS

This work was supported by the Wenner-Gren foundation, OeAD, Austrian Science Foundation (FWF), the Swedish Research Council, KAW foundation, Swedish Energy Agency, the Czech Science Foundation grant GACR 205/10/0989, and the Ministry of Education, Youth, and Sports of the Czech Republic, Grant MEB 061107.

REFERENCES

(1) Davydov, A. S. *Biology and Quantum Mechanics*; Pergamon Press: New York, 1981.
(2) van Amerongen, H.; Valkunas, L.; van Grondelle, R. *Photosynthetic Excitons*; World Scientific: Singapore, 2000.
(3) Kühn, O.; Sundström, V.; Pullerits, T. *Chem. Phys.* **2002**, *275*, 15.
(4) Engel, G. S.; Calhoun, T. R.; Read, E. L.; Ahn, T.-K.; Mančal, T.; Cheng, Y.-C.; Blankenship, R. E.; Fleming, G. R. *Nature* **2007**, *446*, 782.
(5) Ishizaki, A.; Fleming, G. R. *Proc. Natl. Acad. Sci. U.S.A.* **2009**, *106*, 17255.
(6) Hayes, D.; Wen, J.; Panitchayangkoon, G.; Blankenship, R. E.; Engel, G. S. *Faraday Discuss.* **2011**, *150*, 459.
(7) Calhoun, T. R.; Ginsberg, N. S.; Schlau-Cohen, G. S.; Cheng, Y.-C.; Ballottari, M.; Bassi, R.; Fleming, G. R. *J. Phys. Chem. B* **2009**, *113*, 16291.
(8) Collini, E.; Wong, C. Y.; Wilk, K. E.; Curmi, P. M. G.; Brumer, P.; Scholes, G. D. *Nature* **2010**, *463*, 644.
(9) Chen, L.; Zheng, R.; Jing, Y.; Shi, Q. *J. Chem. Phys.* **2011**, *134*, 194508.
(10) Hein, B.; Kreisbeck, C.; Kramer, T.; Rodriguez, M. *New J. Phys.* **2012**, *14*, 023018.
(11) Nalbach, P.; Braun, D.; Thorwart, M. *Phys. Rev. E* **2011**, *84*, 041926.
(12) Abramavicius, D.; Mukamel, S. *J. Chem. Phys.* **2011**, *134*, 174504.
(13) Caycedo-Soler, F.; Chin, A. W.; Almeida, J.; Huelga, S. F.; Plenio, M. B. *J. Chem. Phys.* **2012**, *136*, 155102.
(14) Olbrich, C.; Strumpfer, J.; Schulten, K.; Kleinekathofer, U. *J. Phys. Chem. B* **2011**, *115*, 758.
(15) Shim, S.; Rebentrost, P.; Valleau, S.; Aspuru-Guzik, A. *Biophys. J.* **2012**, *102*, 649−660.
(16) May, V.; Kühn, O. *Charge and Energy Transfer Dynamics in Molecular Systems*; Wiley-VCH: Berlin, 2001.
(17) Adolphs, J.; Renger, T. *Biophys. J.* **2006**, *91*, 2778.
(18) Christensson, N.; Milota, F.; Hauer, J.; Sperling, J.; Bixner, O.; Nemeth, A.; Kauffmann, H. *J. Phys. Chem. B* **2011**, *115*, 5383.
(19) Wendling, M.; Pullerits, T.; Przyjalgowski, M. A.; Vulto, S. I. E.; Aartsma, T. J.; van Grondelle, R.; van Amerongen, H. *J. Phys. Chem. B* **2000**, *104*, 5825.
(20) Rätsep, M.; Freiberg, A. *J. Lumin.* **2007**, *127*, 251−259.
(21) Shelly, K. R.; Carson, E. A.; Beck, W. F. *J. Am. Chem. Soc.* **2003**, *125*, 11810−11811.
(22) Polyutov, S.; Kuhn, O.; Pullerits, T. *Chem. Phys.* **2012**, *394*, 21.
(23) Womick, J. M.; Moran, A. M. *J. Phys. Chem. B* **2011**, *115*, 1347−1356.
(24) Seibt, J.; Renziehausen, K.; Voronine, D. V.; Engel, V. *J. Chem. Phys.* **2009**, *130*, 134318.
(25) Philpott, M. R. *J. Chem. Phys.* **1971**, *55*, 2039.
(26) Spano, F. C. *J. Chem. Phys.* **2002**, *116*, 5877.
(27) Roden, J.; Schulz, G.; Eisfeld, A.; Briggs, J. *J. Chem. Phys.* **2009**, *131*, 044909.
(28) Mukamel, S. *Principles of Nonlinear Optical Spectroscopy*; Oxford University Press: Oxford, U.K., 1995.
(29) Zhang, W. M.; Meier, T.; Chernyak, V.; Mukamel, S. *J. Chem. Phys.* **1998**, *108*, 7763.
(30) Tronrud, D. E.; Wen, J.; Gay, L.; Blankenship, R. *Photosynth. Res.* **2009**, *100*, 79.
(31) Humphrey, W.; Dalke, A.; Schulten, K. *J. Mol. Graphics* **1996**, *14*, 33.
(32) Czarnecki, K.; Diers, J. R.; Chynwat, V.; Erickson, J. P.; Frank, H. A.; Bocian, D. F. *J. Am. Chem. Soc.* **1997**, *119*, 415−426.
(33) Rätsep, M.; Cai, Z.; Reimers, J. R.; Freiberg, A. *J. Chem. Phys.* **2011**, *134*, 024506.

(34) Panitchayangkoon, G.; Voronine, D.; Abramavicius, D.; Caram, J. R.; Lewis, N. H. C.; Mukamel, S.; Engel, G. S. *Proc. Natl. Acad. Sci. U.S.A.* **2011**, *108*, 20908.
(35) Caram, J. R.; Engel, G. S. *Faraday Discuss.* **2011**, *153*, 93−104.